ARTICLE

Six-Dimensional *ab initio* Potential Energy Surface and Bound States for He-H_2S Complex

Chao-ying Han[a], Ting Jiang[a], Hua Zhu[a*], Hong-jun Fan[b*]

a. School of Chemistry, Sichuan University, Chengdu 610064, China
b. School of Biological Engineering, Sichuan University of Science & Engineering, Zigong 643000, China

(Dated: Received on July 27, 2019; Accepted on October 16, 2019)

We present a new six-dimensional potential energy surface for He-H_2S including the intramolecular Q_1, Q_2, and Q_3 normal modes for the ν_1 symmetric stretching, ν_2 bending and ν_3 asymmetric stretching of H_2S. The potential was calculated at the coupled-cluster singles and doubles with noniterative inclusion of connected triples [CCSD(T)]-F12a level with augmented correlation-consistent polarized-valence triple-zeta (aug-cc-pVTZ) basis set plus the midpoint bond function (3s3p2d1f1g). Three vibrationally averaged potentials with H_2S at the vibrational ground state ν_1 as well as the excited states ν_2 and ν_3 were generated from the integration of the six-dimensional potential over the Q_1, Q_2 and Q_3 coordinates. Each potential has a planar T-shaped global minimum, a planar local minimum, two in-plane saddle points as well as an out-plane saddle point. The global minimum is located at R=3.46 Å, θ=109.9° and φ=0.0° with a well depth of 35.301 cm^{-1}. The radial discrete variable representation/angular finite basis representation method and the Lanczos algorithm were employed to calculate the rovibrational energy levels. The calculated band origins are blue-shifted (0.025 cm^{-1} and 0.031 cm^{-1}) and (0.041 cm^{-1} and 0.060 cm^{-1}) for He-(*para*-H_2S) and He-(*ortho*-H_2S) in the ν_2 and ν_3 region of the H_2S molecule, respectively.

Key words: He-H_2S, Potential energy surface, Bound state

I. INTRODUCTION

Van der Waals (vdW) complexes between rare-gas (Rg) atoms and nonlinear H_2X (X=O, S) molecules are of considerable interest in recent years. Such researches have been aimed at understanding the nature of the weak intermolecular potentials and dynamics of these weakly bound complexes. H_2O is one of the most significant interstellar molecules and is a key element in biological systems and collision phenomena [1−4], so considerable experimental and theoretical studies have been devoted to determining such potentials and rovibrational spectra in prototype systems formed by H_2O and Rg atoms. Compared with H_2O, H_2S also plays an equally important role in chemistry and in the spectroscopy of giant planets [5, 6]. It is intriguing to explore the difference of structure and dynamical features between the H_2S containing complexes and the H_2O containing analogues.

Many experimental researches have been carried out concerning the Rg-H_2O complexes [7−14]. In 1988, Cohen *et al.* first studied the infrared spectra of the Ar-H_2O complex in the region of the H_2O asymmetric stretching ν_3 fundamental band using a tunable infrared laser [7]. The results showed that the complex has a hydrogen bonded equilibrium structure. Subsequently, further experimental studies of microwave and infrared spectra for Rg-H_2O (Rg=Ne, Ar, Kr, Xe) were reported [8−14]. For the complexes involving H_2S, available experimental information is limited to the microwave spectra of Ar-H_2S [15, 16] and Ne-H_2S [17]. In 1997, the rotational spectra, structure, and internal dynamics of various isotopomers of the Ar-H_2S dimer has been investigated by Gutowsky *et al.* [16]. Later Liu *et al.* [17] measured the rotational spectra of 15 isotopic species and internal dynamics of Ne-H_2S. The above experimental researches revealed that these Rg-H_2S complexes have a planar T-shaped structure similar to that of the Rg-H_2O complexes.

Along with these experimental researches, a number of theoretical studies [18−30] have dealt with the construction of the *ab initio* potential energy surface. The first *ab initio* potential for Ar-H_2O [18] was reported via employing the second-order many-body perturbation theory. Subsequently, further investigations of potential energy surfaces for Rg-H_2O [22, 23] (Rg=He, Ne, Ar, Kr, Xe) were carried out at the coupled-cluster singles and doubles with noniterative inclusion of connected triples [CCSD(T)] level. For the complexes inv-

*Authors to whom correspondence should be addressed. E-mail: zhuhua@scu.edu.cn, hjfan@suse.edu.cn

olving H_2S, Oliveira *et al.* [24] proposed a potential energy surface which was limited to the region around equilibrium structure using MP2 method for Ar-H_2S in early time. Later, extensive *ab initio* calculations were carried out for Ne-H_2S [26] and Ar-H_2S [27] adopting aug-cc-pVQZ basis set at [CCSD(T)] level, the rovibrational bound states and microwave spectra for these complexes were studied based on the potential energy surfaces. In the above researches, H_2O or H_2S molecule was treated as a rigid rotor, which was sufficient for describing microwave spectra of ground-state species, but not enough for predicting the infrared spectra including the transition in the intramolecular vibrational modes. An improved approach was to construct the potential by explicitly involving the dependence of the intramolecular vibrational coordinates [31]. Up to now, the six-dimensional potential energy surfaces for Rg-H_2O (Rg=He, Ne, Ar) containing the intramolecular Q_1, Q_2, and Q_3 vibrational modes for the ν_1 symmetric stretching vibration, ν_2 bending vibration and ν_3 asymmetric stretching vibration of H_2O have been presented based on this method [28−30].

To the best of our knowledge, there is still no reliable intermolecular potential energy surface for He-H_2S which includes the intramolecular vibration modes of the H_2S monomer. The available potential for He-H_2S [25] was calculated with rigid monomer model, also not sufficient for the bound state calculations, because it was only limited to the region of the potential well. And it was only discussed on one-dimensional energy curves of the interaction energy as the function of distance R or angle θ (E-R or E-θ). Recently, we have successfully constructed a full six-dimensional potential energy surface for the Ar-H_2S [32] system that explicitly depends on the three intramolecular vibrational modes of H_2S. The calculated infrared spectra for Ar-(*para*-H_2S) and Ar-(*ortho*-H_2S) are in good agreement with the experimental results. In the present work, a new six-dimensional potential for He-H_2S is presented, and is expected to be as accurate as that for Ar-H_2S. Using the obtained potential, we first predict the rovibrational spectra of He-(*para*-H_2S) and He-(*ortho*-H_2S), respectively. And we hope that the regularity of potential energy surfaces, rovibrational bound states, band origin shifts, as well as the effect of the intramolecular normal modes on the potentials and rovibrational spectra can be explored for the series of Rg-H_2S dimers.

The six-dimensional *ab initio* potential for He-H_2S was constructed using [CCSD(T)]-F12a method with a large basis set plus bond functions. The Q_1, Q_2, and Q_3 normal modes for the symmetric stretching, bend and antisymmetric stretching vibration of H_2S were included in the construction of the potential. The potential optimized discrete variable representation (PODVR) [33] grid points were used to construct intermolecular potential energy surface. The combined radial discrete variable representation (DVR)/angular finite basis representation (FBR) method and Lanczos algorithm were used to calculate the rovibrational energy levels and the bound states.

II. COMPUTATIONAL DETAILS

A. *Ab initio* calculations

The geometry of He-H_2S can be described by the body-fixed Jacobi coordinates (R, θ, φ, Q, Q_2, Q_3): R stands for the distance from the He atom to the center of mass of H_2S, θ denotes the angle between the **R** vector and the C_2 axis of H_2S, and φ is the dihedral angle between the two planes defined by **R** vector with C_2 and the H_2S molecule plane. The intramolecular coordinates Q_1, Q_2, and Q_3 represent the ν_1 symmetric stretching, ν_2 bending, and ν_3 asymmetric stretching vibration of H_2S, respectively. We adopted PODVR grid points in our latest work of Ar-H_2S [32] for the three coordinates.

The potential energies for He-H_2S were calculated with R ranging from 2.40 Å to 10.00 Å, angles θ from 0.0° to 180.0° in a step of 15.0°, and φ from 0.0° to 90.0° at intervals of 30.0°. The calculations of potential energies were performed at the [CCSD(T)]-F12a level. The aug-cc-pVTZ basis set of Woon and Dunning [34] was employed for all atoms plus midpoint bond functions (3s3p2d1f1g) [35]. [CCSD(T)]-F12a/aVTZ can provide a remarkable description of the intermolecular interaction energies [36, 37]. The full counterpoise procedure [38] was used to correct for the basis set superposition error (BSSE). According to it, the energies of monomers are calculated using the same full basis set. All *ab initio* calculations were carried out using the MOLPRO package [39].

The effective potentials $V_{\nu_1,\nu_2,\nu_3}(R,\theta,\varphi)$ with H_2S at the vibrational ground state as well as the ν_2 and ν_3 excited states were acquired by averaging the six-dimensional potential over the intramolecular Q_1, Q_2, and Q_3 vibrational coordinates.

$$\begin{aligned} &V_{\nu_1,\nu_3}(R,\theta,\varphi,Q_2) \\ &= \int_{-\infty}^{\infty} \big[\psi^*_{\nu_1,\nu_3}(Q_1,Q_3)\cdot V(R,\theta,\varphi,Q_1,Q_2,Q_3)\cdot \\ &\qquad \psi_{\nu_1,\nu_3}(Q_1,Q_3)\mathrm{d}Q_1\mathrm{d}Q_3\big] \end{aligned} \tag{1}$$

$$\begin{aligned} &V_{\nu_1,\nu_2,\nu_3}(R,\theta,\varphi) \\ &= \int_{-\infty}^{\infty} \psi^*_{\nu_2}(Q_2)\cdot V_{\nu_1,\nu_3}(R,\theta,\varphi,Q_2)\cdot \psi_{\nu_2}(Q_2)\mathrm{d}Q_2 \end{aligned} \tag{2}$$

In which vibrational wave functions in Eq.(1) and Eq.(2) were determined by calculating the two-dimensional $V_{H_2S}(Q_1,Q_3)$ and one-dimensional $V_{H_2S}(Q_2)$ potentials. The intramolecular potential energy surface of $V_{H_2S}(Q)$ governing the Q_1, Q_2, and Q_3 vibration of the isolated H_2S monomer was determined by Kozin *et al.* [40] from experimental spectroscopic data. The averaged intermolecular potentials $V_{\nu_1,\nu_2,\nu_3}(R,\theta,\varphi)$ were fitted to a three-dimensional

DOI:10.1063/1674-0068/cjcp1907145

Morse/Long-Range (MLR) potential function employing the identical approach as Ref.[28].

B. Calculations of the rovibrational bound states

Within the Born-Oppenheimer approximation, the vibrational averaged intermolecular Hamiltonian of He-H_2S can be expressed as [29, 32]

$$\hat{H} = -\frac{1}{2\mu}\frac{\partial^2}{\partial R^2} + \frac{1}{2\mu R^2}(\hat{J}-\hat{j})^2 + \hat{H}_{\mathrm{H_2S}} + V_{\nu_1,\nu_2,\nu_3}(R,\theta,\varphi) \quad (3)$$

where μ is the reduced mass of He-H_2S, $\hat{J}$ and $\hat{j}$ are the angular momentum operators corresponding to the total and the H_2S monomer rotations, respectively, and $\hat{H}_{\mathrm{H_2S}}$ represents the rigid rotor kinetic energy operator for H_2S.

$$\hat{H}_{\mathrm{H_2S}} = \left(\frac{A+C}{2}\right)\hat{j^2} + \left[B - \left(\frac{A+C}{2}\right)\right]\hat{j_z^2} + \left(\frac{A-C}{4}\right)\left(\hat{j_+^2} + \hat{j_-^2}\right) \quad (4)$$

where A, B, and C are the rotational constants of H_2S [41], and $\hat{j_\pm}=\hat{j_x} \mp i\hat{j_y}$.

The rovibrational bound states and energy levels were calculated with the effective radial DVR/angular FBR method [42, 43]. In our calculations, we used 60 sine-DVR [44] points for the R coordinate, 26 Gauss-Legendre grid points and 26 Gauss-Chebyshev quadrature points for the numerical integration over θ and φ. The Lanczos algorithm [45] was employed to efficiently diagonalize the Hamiltonian matrix. For the angular coordinates, the parity-adapted rotational basis function $\Theta_{jk}^{JMK\varepsilon}$ was defined in the following form [21, 22],

$$\Theta_{jk}^{JMK\varepsilon} = \frac{1}{\sqrt{2(1+\delta_{K0}\delta_{k0})}}[D_{MK}^{J^*}(\alpha,\beta,\gamma)D_{Kk}^{j^*}(0,\theta,\varphi) + \varepsilon(-1)^{J+k}D_{M-K}^{J^*}(\alpha,\beta,\gamma)D_{-K-k}^{j^*}(0,\theta,\varphi)] \quad (5)$$

$D_{MK}^{J^*}$ and $D_{Kk}^{j^*}$ are the normalized rotational functions to describe the overall rotation of the complex and the rotation of the H_2S molecular, respectively.

III. THE CHARACTERISTICS OF POTENTIAL ENERGY SURFACES

The root-mean-square (rms) error between the fitted and the calculated points was found to be 0.1 cm^{-1}. The FORTRAN subroutine for generating potential energy surface of He-H_2S can be seen in the supplementary material. The 3D potentials were obtained by fitting parameters. The contour plots of the averaged potential energy surface of He-H_2S with H_2S at the vibrational ground state are shown in FIG. 1. One can see that the potential exhibits a large angular anisotropy and a strong radial-angular coupling. FIG. 1(a) presents how the minimum potential depends on θ and R when φ=0.0°. The global minimum (point A) with the well depth of 35.301 cm^{-1} is located at R=3.46 Å, θ=109.9° and φ=0.0°, which is in a planar T-shape geometry with He in the H_2S molecular plane (φ=0.0°). A planar local minimum (point B) with a well depth of 26.072 cm^{-1} occurs at R=3.87 Å and θ=0.0°. The saddle point (point C) connecting the two minima was found to be a planar structure at R=4.18 Å and θ=44.2° with the barriers height of 14.720 cm^{-1}, relative to the global minimum. In addition, another planar first-order saddle point (point D) is located at R=3.77 Å and θ=180.0° with the barriers height of 14.519 cm^{-1} with respect to the global minimum. FIG. 1(b) shows the contour plot of the potential energy surface of He-H_2S with R fixed at its equilibrium value of 3.46 Å. Due to the symmetry of the system, φ direction is only displayed in the range from 0.0° to 180.0°. A second-order saddle point is for the out-plane rotation which is hindered by a barrier of 22.598 cm^{-1} at R=4.15 Å, θ=88.4° and φ=90.0°, relative to the global minimum.

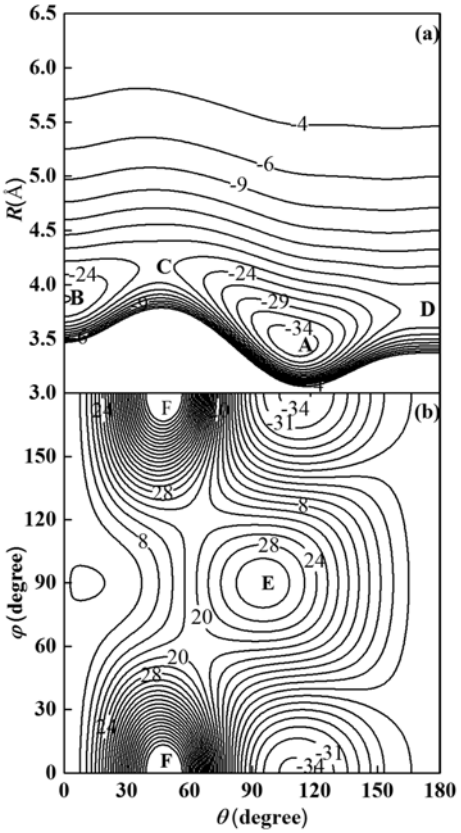

FIG. 1 Contour plots of the potential energy surface for He-H_2S with H_2S at the vibrational ground state: (a) φ is fixed at 0.0°, and (b) R is fixed at 3.46 Å.

The characteristic points and their corresponding en-

DOI:10.1063/1674-0068/cjcp1907145

TABLE I Characteristic points (R in Å, θ and φ in degree) and the well depths (in cm^{-1}) of the He-H_2S with H_2S at the vibrational ground and excited states.

State	Global minimum	Local minimum	In-plane barriers
He-H_2S(0,0,0)	{3.46, 109.9, 0.0, −35.301}	{3.87, 0.0, 0.0, −26.072}	{4.18, 44.2, 0.0, −20.581}
			{3.77, 180.0, 0.0, −20.782}
He-H_2S(0,1,0)	{3.47, 110.1, 0.0, −35.150}	{3.87, 0.0, 0.0, −26.161}	{4.18, 43.9, 0.0, −20.410}
			{3.77, 180.0, 0.0, −20.821}
He-H_2S(0,0,1)	{3.47, 110.0, 0.0, −35.201}	{3.93, 0.0, 0.0, −24.902}	{4.21, 42.7, 0.0, −19.831}
			{3.79, 180.0, 0.0, −20.920}

ergies for the effective three-dimensional potentials for He-H_2S with H_2S at the vibrational ground state as well as ν_2 and ν_3 excited states are listed in Table I. The variation values of each stationary point are extremely small at different states of H_2S. FIG. 2 presents distance R_m and the minimum potentials V_m along the minimum potential path for He-H_2S at the ground and excited states of H_2S. It is clear that the contour plot at the ground state looks the same as that for the excited states. For comparison between He-H_2S and Ar-H_2S [32], the interaction between He and H_2S is weaker than that between Ar and H_2S, the well depth of He-H_2S is 143.939 cm^{-1} significantly shallower than that of Ar-H_2S. In addition, there are obvious differences in the stationary points between the two complexes. For example, the distances R for all stationary geometries of He-H_2S are about 0.30 Å larger than those of Ar-H_2S, and deviations of angular coordinate θ are about 5.0°.

The He-H_2O equilibrium structure employs a hydrogen bonded position [29], whereas an anti-hydrogen bonded orientation is adopted for He-H_2S, though the two complexes are found to have the T-shaped global geometry, and the global minimum for He-H_2S is only 1.212 cm^{-1} deeper than that for He-H_2O. Compared with He-H_2O, the R coordinates of each stationary point for He-H_2S are about 0.40 Å larger than those of He-H_2O, which may be mainly derived from the larger atomic radius of the sulfur atom. As we all know, He-H_2O has only one planar global minimum, while He-H_2S has an additional planar local minimum, In contrast to the case of He-H_2O, the He-H_2S potential presents a local minimum in the planar configuration (θ=0.0°, φ=0.0°), rather than the first-order saddle point found for the He-H_2O complex.

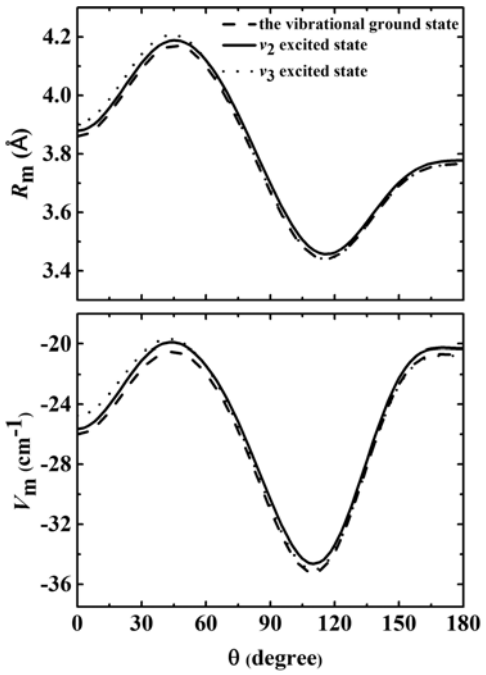

FIG. 2 Radial position (upper) and energy (lower) along the minimum energy path for He-H_2S with H_2S at the vibrational ground state as well as the ν_2 and ν_3 excited states as functions of angle θ for optimized values of φ and R.

IV. BOUND STATES AND ROVIBRATIONAL ENERGY LEVLES

The calculated rovibrational bound states were marked with six quantum numbers (J, K, j, k, P, n_s) in free internal rotor model, where J represents the total angular momentum number, K is the projection of total angular momentum J on the BF z-axis, states with K=0, or K=1 are represented by Greek capital letter Σ or Π state, $j_{k_a k_c}$ means asymmetric top level of the H_2S subunit, k denotes the projection of j on the C_2 axis of the H_2S monomer where the evenness and oddness of determine whether they belong to the He-(*para*-H_2S) or He-(ortho-H_2S) complex, P shows the parity e or f symmetry with $P=(-1)^J$ or $P=(-1)^{J+1}$, and quantum number n_s represents the intermolecular stretching mode.

The calculated rovibrational energy levels within $J\leq 4$ for He-(*para*-H_2S) and He-(*ortho*-H_2S) with H_2S at the vibrational ground state as well as ν_2 and ν_3 excited states are listed in Table II. One can see the rovibrational energy levels of the three states are almost identical. Our potentials support only one vibrational bound state for both He-(*para*-H_2S) and He-(*ortho*-H_2S). The lowest vibrational energy of −7.161 cm^{-1} for He-(*para*-H_2S) with H_2S at the vibrational ground state corre-

DOI:10.1063/1674-0068/cjcp1907145

TABLE II The calculated energy levels for He-H_2S with H_2S at the vibrational ground and excited states (labeled with $K(j_{k_a k_c})^{J+P}$). The * means resonance states.

	Vibrational energy/cm^{-1}					State
	J=0	J=1	J=2	J=3	J=4	
He-(*para*-H_2S) (0,0,0)	−7.161	−6.674	−5.708	−4.286	−2.421	$\Sigma(0_{00})^e$
		7.699	8.168	9.437	10.716	$^*\Pi(1_{11})^e$
		8.559	9.524	10.951	12.804	$\Pi(1_{11})^f$
He-(*ortho*-H_2S) (0,0,0)	5.702	5.938	6.547	7.593	9.087	$\Sigma(1_{01})^e$
		7.931	9.261	11.075	13.292	$\Pi(1_{01})^e$
		7.663	8.601	9.984	11.782	$\Pi(1_{01})^f$
He-(*para*-H_2S) (0,1,0)	−7.136	−6.689	−5.725	−4.299	−2.442	$\Sigma(0_{00})^e$
		7.910	8.893	9.636	10.983	$^*\Pi(1_{11})^e$
		8.847	9.811	11.236	13.090	$\Pi(1_{11})^f$
He-(*ortho*-H_2S) (0,1,0)	5.743	6.084	6.688	7.730	9.220	$\Sigma(1_{01})^e$
		8.056	9.387	11.202	13.419	$\Pi(1_{01})^e$
		7.784	8.721	10.104	11.902	$\Pi(1_{01})^f$
He-(*para*-H_2S) (0,0,1)	−7.130	−6.607	−5.646	−4.225	−2.375	$\Sigma(0_{00})^e$
		7.515	7.979	8.847	10.546	$^*\Pi(1_{11})^e$
		8.320	9.283	10.708	12.556	$\Pi(1_{11})^f$
He-(*ortho*-H_2S) (0,0,1)	5.762	5.882	6.487	7.528	9.014	$\Sigma(1_{01})^e$
		7.862	9.186	10.992	13.196	$\Pi(1_{01})^e$
		7.595	8.528	9.905	11.693	$\Pi(1_{01})^f$

TABLE III The rovibrational energy comparison for He-H_2S on the $\Sigma(0_{00})^e$ and $\Sigma(1_{01})^e$ states with H_2S at the vibrational ground and excited states (in cm^{-1}).

	Rovibrational energy on $\Sigma(0_{00})^e$ state/cm^{-1}			Rovibrational energy on $\Sigma(1_{01})^e$ state/cm^{-1}		
	He-H_2S(0,0,0)	He-H_2S(0,1,0)	He-H_2S(0,0,1)	He-H_2S(0,0,0)	He-H_2S(0,1,0)	He-H_2S(0,0,1)
J=0	−7.161	−7.136	−7.130	5.702	5.743	5.762
J=1	−6.674	−6.689	−6.607	5.938	6.084	5.882
J=2	−5.708	−5.725	−5.646	6.547	6.688	6.487
J=3	−4.286	−4.299	−4.225	7.593	7.730	7.528
J=4	−2.421	−2.442	−2.375	9.087	9.220	9.014

sponds to the zero-point energy of 28.140 cm^{-1}, which is about 80% of the well depth (35.301 cm^{-1}). The zero-point energy is distinctly higher than the in-plane barrier height of 14.720 and 14.519 cm^{-1}. With such lower barriers, the minima are not able to trap the He atom very well, leading to a delocalized angular distribution. In the case of He-(*ortho*-H_2S), the energy level for a bound state of the complex is that the total rovibrational energy minus the rotational energy for the free H_2S molecule. The asymptote for *ortho*-H_2S with $j_{k_a k_c}$=1_{01} had the energy of 13.749 cm^{-1} [46], which was calculated from the sum of the rotational constants B+C of H_2S. As seen in Table II, the lowest vibrational energy is 5.702 cm^{-1}, corresponding to the truly bound state energy of −8.047 cm^{-1}, so the zero-point energy is 27.254 cm^{-1} for He-(*ortho*-H_2S), which is about 1 cm^{-1} lower than that of He-(*para*-H_2S). Table III presents the energy levels on the lowest two states $\Sigma\,(0_{00})^e$ and $\Sigma\,(1_{01})^e$ for He-H_2S with H_2S at the vibrational ground state as well as ν_2 and ν_3 excited states. The predicted vibrational band origins are blue-shifted by 0.025 cm^{-1} and 0.031 cm^{-1} for He-(*para*-H_2S) in the ν_2 and ν_3 region of H_2S, respectively. For the He-(*ortho*-H_2S) complex, the predicted vibrational band origins are also blue-shifted by 0.034 cm^{-1} and 0.060 cm^{-1} with H_2S at the ν_2 and ν_3 states, respectively. The smaller H_2S band origin shifts reveal a slight weakening of the vdW bond upon vibration excitation for He-H_2S. Compared with He-H_2S, the shifts for Ar-H_2S [32] are larger (−0.38 and −0.63 cm^{-1}). The shifts of the two complexes are consistent with a common trend that the lighter, less-polarizable partner He tends to induce positive (blue-shifted), while the heavier, polarizable partner Ar tends to move these shifts to the red.

To further research the properties of the vibrational states, it is necessary to visualize the wave functions. FIG. 3 and FIG. 4 present the contour plots of wave

DOI:10.1063/1674-0068/cjcp1907145

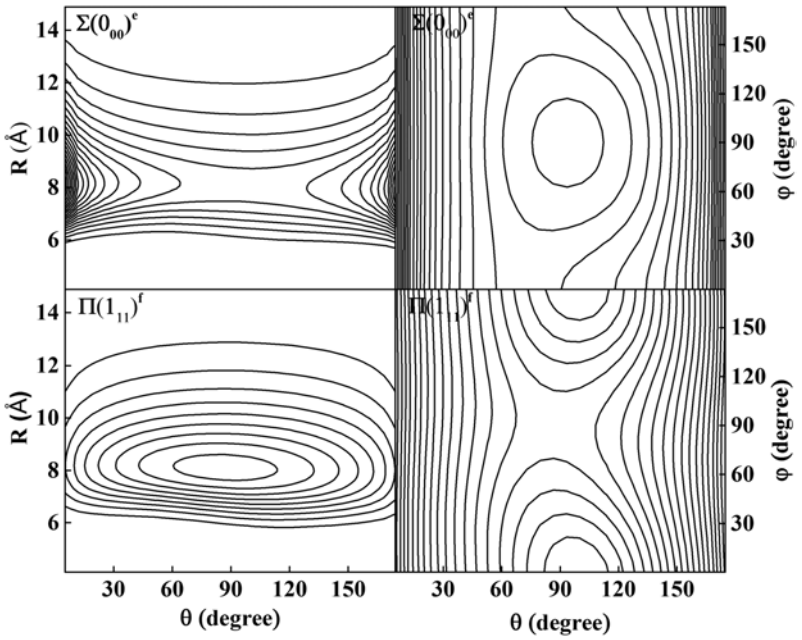

FIG. 3 The wave functions for the lower energy levels of He-(*para*-H_2S): (left panel) as a function of R and θ, (right panel) as a function of θ and φ, respectively.

functions for some lower rovibrational energy levels of He-(*para*-H_2S) and He-(*ortho*-H_2S) with H_2S at the vibrational ground state, respectively. It is clear that these states spread over the entire range of angles. For comparison between the wave functions of He-(*para*-H_2S) and those of He-(*ortho*-H_2S), the variation of wave functions of $\theta-\varphi$ is very small along φ coordinate for He-(*para*-H_2S), while the variation of wave functions of $\theta-\varphi$ is remarkable along φ coordinate for He-(*ortho*-H_2S). For He-(*para*-H_2S), the analysis of the wave functions indicated that $\Pi\,(1_{11})^{\rm e}$ is a resonance state, and the Π-contributions of $\Pi\,(1_{11})^{\rm f}$ state accounts for 58%, 57%, 43%, and 71% for J=1, 2, 3 and 4, respectively, while the $\Pi\,(1_{11})^{\rm f}$ state has 99% of Π-contribution for J=1−4. For He-(*ortho*-H_2S), the wave function on the $\Sigma\,(1_{01})^{\rm e}$ state only exhibits a clear node along coordinate, the wave functions on the $\Pi\,(1_{01})^{\rm e}$ and $\Pi\,(1_{01})^{\rm f}$ states also show the clear nodal structure along θ and φ coordinates, and the two states display strong coupling between θ and φ coordinates.

V. CONCLUSION

In this work, an accurate six-dimensional potential energy surface for He-H_2S which explicitly involves the intramolecular Q_1, Q_2 and Q_3 normal coordinates for the ν_1 symmetric stretching vibration, ν_2 bending vibration and ν_3 asymmetric stretching vibration of H_2S was presented. The intermolecular potential was calculated over five PODVR grid points for the Q_1, Q_2, and Q_3 normal modes, respectively, employing the [CCSD(T)]-F12a method with aug-cc-pVTZ basis set plus bond functions placed at the mid-point on the intermolecular axis. Three vibrationally averaged potential energy surfaces of He-H_2S with H_2S at the vibrational ground state as well as the ν_2 and ν_3 excited states were generated from averaging of the six-dimensional potential over the Q_1, Q_2, and Q_3 coordinates. It was found that each averaged potential energy surface has a T-shaped global minimum, a planar local minimum, two in-plane saddle points and an out-plane saddle point. Based on the *ab initio* potentials, rovibrational energy levels were calculated using the radial DVR/angular FBR method for He-(*para*-H_2S) and He-(*ortho*-H_2S) with H_2S at different states. Our potentials support only one vibrational bound state for He-(*para*-H_2S) and He-(*ortho*-H_2S), respectively. In addition, we predicted that the band origins were blue-shifted (0.025 cm^{-1} and 0.031 cm^{-1}) and (0.041 cm^{-1} and 0.060 cm^{-1}) for He-(*para*-H_2S) and He-(*ortho*-H_2S) with the H_2S molecule at the ν_2 and ν_3 states, respectively. It is expected that the potential energy surfaces and rovibrational bound states should be useful for further theoretical and experimental studies for the He-H_2S complex.

Supplementary materials: The FORTRAN subroutine which generates potential energy surfaces of He-H_2S can be found.

VI. ACKNOWLEDGMENTS

This work was supported by the National Natural Science Foundation of China (No.21973065) and Sichuan

DOI:10.1063/1674-0068/cjcp1907145

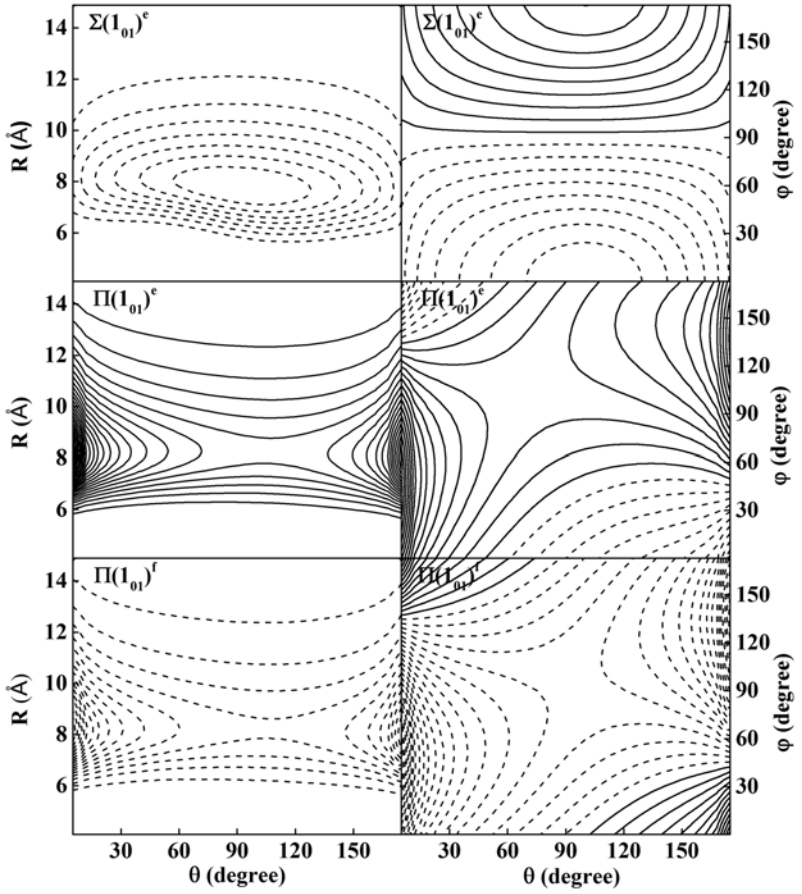

FIG. 4 The wave functions for the lower energy levels of He-(*ortho*-H_2S). Left panel: as functions of R and θ, right panel: as functions of θ and φ, respectively.

Science and Technology Program (No.2018JY0172).

[1] R. Lascola and D. J. Nesbitt, J. Chem. Phys. **95**, 7917 (1991).
[2] S. Hirabayashi and K. M. T. Yamada, Chem. Phys. **Lett**. 418, 323 (2006).
[3] B. Yang and P. C. Stancil, J. Chem. Phys. **126**, 154306 (2007).
[4] B. Yang, M. Nagao, W. Satomi, M. Kimura, and P. C. Stancil, Astrophys. J. **765**, 77 (2013).
[5] J. M. Flaud and C. Camy-Peyr, Can. J. Phys. **61**, 1462 (1983).
[6] R. P. Wayne, *Chemistry of Atmospheres*, Oxford, UK: Clarendon Press, (1991).
[7] R. C. Cohen, K. L. Busarow, K. B. Laughlin, G. A. Blake, M. Havenith, Y. T. Lee, and R. J. Saykally, J. Chem. Phys. **89**, 4494 (1988).
[8] G. T. Fraser, F. J. Lovas, R. D. Suenram, and K. Matsumura, J. Mol. Spectros. **144**, 97 (1990).
[9] R. C. Cohen, K. L. Busarow, Y. T. Lee, and R. J. Saykally, J. Chem. Phys. **92**, 169 (1990).
[10] D. J. Nesbitt and R. Lascola, J. Chem. Phys. **97**, 8096 (1992).
[11] R. C. Cohen and R. J. Saykally, J. Chem. Phys. **98**, 6007 (1993).
[12] J. V. Wijngaarden, and W. Jäger, Mol. Phys. **98**, 1575 (2000).
[13] Q. Wen and W. Jäger, J. Phys. Chem. A **110**, 7560 (2006).
[14] S. Li, R. Zheng, Y. Zhu, and C. X. Duan, J. Chem. Phys. **135**, 134304 (2011).
[15] R. Viswanathan and T. R. Dyke, J. Chem. Phys. **82**, 1674 (1985).
[16] H. S. Gutowsky, T. Emilsson, and E. Arunan, J. Chem. Phys. **106**, 5309 (1997).
[17] Y. Liu and W. Jäger, Mol. Phys. **100**, 611 (2002).
[18] G. Chal/asiński, M. M. Szczęśniak, and S. Scheiner, J. Chem. Phys. **94**, 2807 (1991).
[19] M. Bulski, P. E. S. Wormer, and A. van der Avoird, J. Chem. Phys. **94**, 8096 (1991).
[20] K. Patkowski, T. Korona, R. Moszynski, B. Jeziorski, and K. Szalewicz, J. Mol. Struct. **591**, 231 (2002).
[21] X. L. Sun, Y. Hu, and H. Zhu, J. Chem. Phys. **138**, 204312 (2013).
[22] J. Makarewicz, J. Chem. Phys. **129**, 184310 (2008).
[23] L. Wang and M. H. Yang, J. Chem. Phys. **129**, 174305 (2008).
[24] G. de Oliveira and C. E. Dykstra, J. Chem. Phys. **106**, 5316 (1997).

DOI:10.1063/1674-0068/cjcp1907145

[25] D. Cappelletti, A. F. Vilela, P. R. Barreto, R. Gargano, F. Pirani, and V. Aquilanti, J. Chem. Phys. **125**, 133111 (2006).
[26] J. P. Lei, M. Y. Xiao, Y. Z. Zhou, and D. Q. Xie, J. Chem. Phys. **136**, 214307 (2012).
[27] J. P. Lei, Y. Z. Zhou, and D. Q. Xie, J. Chem. Phys. **136**, 084310 (2012).
[28] D. Hou, Y. T. Ma, X. L. Zhang, and H. Li, J. Chem. Phys. **144**, 014301 (2016).
[29] D. Hou, Y. T. Ma, X. L. Zhang, and H. Li, J. Mol. Spectrosc. **330**, 217 (2016).
[30] X. Liu, D. Hou, J. Thomas, H. Li, and Y. Xu, J. Mol. Spectrosc. **330**, 236 (2016).
[31] H. Guo, R. Q. Chen, and D. Q. X, J. Theo. Comput. Chem. **1**, 173 (2002).
[32] T. Jiang, C. Y. Han, and H. Zhu, Mol. Phys. **118**, e1612958 (2020).
[33] H. Wei and T. Carrington, J. Chem. Phys. **97**, 3029 (1992).
[34] D. E. Woon and T. H. Dunning, J. Chem. Phys. **98**, 1358 (1993).
[35] T. B. Pedersen and B. Fernández, J. Chem. Phys. **115**, 8431 (2001).
[36] T. Yuan and H. Zhu, Theor. Chem. Acc. **133**, 1 (2014).
[37] J. M. Liu, Y. Zhai, and H. Li, J. Chem. Phys. **147**, 044313 (2017).
[38] S. F. Boys and F. Bernardi, Mol. Phys. **19**, 553 (1970).
[39] H. J. Werner, P. J. Knowles, R. D. Amos, A. Berning, D. L. Cooper, M. J. O. Deegan, A. J. Dobbyn, F. Eckert, S. T. Elbert, C. Hampel, R. Lindh, A. W. Lloyd, W. Meyer, A. Nicklass, K. Peterson, R. Pitzer, A. J. Stone, P. R. Taylor, M. E. Mura, P. Pulay, M. Schutz, H. Stoll, and T. Thoorstcinsso, *MOLPRO, version 2000.1, a Package of ab initio Programs 2000.* http://www.molpro.net.
[40] I. N. Kozin and P. Jensen, J. Mol. Spectrosc. **163**, 483 (1994).
[41] Ala'a A. A. Azzam, S. N. Yurchenko, J. Tennyson, M. Aline, M. Drumel, and O. Pirali, J. Quant. Spectrosc. Radiat. Transfer. **130**, 341 (2013).
[42] S. Y. Lin and H. Guo, J. Chem. Phys. **117**, 5183 (2002).
[43] C. Leforestier, J. Chem. Phys. **101**, 7357 (1994).
[44] D. T. Colbert and W. H. Miller, J. Chem. Phys. **96**, 1982 (1992).
[45] C. J. Lanczos, Res. Natl. Bur. Stand. **45**, 255 (1950).
[46] G. Cazzoli and C. Puzzarini, J. Mol. Spectros. **298**, 31 (2014).

DOI:10.1063/1674-0068/cjcp1907145